PRL Heterogeneity in Multiple Sclerosis: Pathophysiological and Clinical Implications

Anna Stölting, M.Sc.,[1] Colin Vanden Bulcke, PhD,[1,2] Serena Borrelli, MD,[1,3] Matthieu Deltombe, MD,[4,5] Jean-Louis Bayart, M.Sc.,[4,6] Eline Van Doninck, M.Sc.,[1,7] Céline Bugli, PhD,[8] Vincent van Pesch, MD, PhD,[5,9] María I. Gaitán, MD,[10] Martina Absinta, MD, PhD,[11,12] Daniel S. Reich, MD, PhD,[10] Pietro Maggi, MD, PhD,[1,9]

Author affiliations:

1 Neuroinflammation Imaging Lab (NIL), Institute of NeuroScience, Université catholique de Louvain, 1200 Brussels, Belgium.

2 ICTEAM Institute, Université catholique de Louvain, 1348 Louvain-la-Neuve, Belgium.

3 Department of Neurology, Hôpital Erasme, Hôpital Universitaire de Bruxelles, Université Libre de Brussels, 1200 Brussels, Belgium.

4 Department of Laboratory Medicine, Cliniques Universitaires Saint-Luc, 1200 Bruxelles, Belgium.

5 Laboratory of Neurochemistry, Institute of NeuroScience, Université catholique de Louvain, 1200 Brussels, Belgium

6 Department of Laboratory Medicine, Clinique St-Pierre, 1340 Ottignies, Belgium

7 University of Antwerp, Department of Family Medicine and Population Health, Faculty of Medicine and Health Sciences, 2610 Wilrijk, Belgium

8 Plateforme technologique de Support en Méthodologie et Calcul Statistique, Université catholique de Louvain, 1200 Brussels, Belgium

9 Department of Neurology, Cliniques universitaires Saint-Luc, Université catholique de Louvain, 1200 Brussels, Belgium

10 Translational Neuroradiology Section, National Institute of Neurological Disorders and Stroke, National Institutes of Health, Bethesda, MD 20892, United States of America

11 Experimental Neuropathology Lab, IRCCS Humanitas Research Hospital, 20089 Milan, Italy

12 Department of Biomedical Sciences, Humanitas University, 20072 Milan, Italy

Manuscript Word Count: 5506

Number of Figures/Tables: 5/1

Number of References: 52

Abstract Word Count: 319

Running title: PRL Heterogeneity in Multiple Sclerosis

Correspondence to: Pietro Maggi

Full address: Avenue Hippocrate 10, 120 Bruxelles, Belgium

E-mail: pietro.maggi@uclouvain.be

Telephone: +32 (0)27648547

Abstract

Background

In multiple sclerosis (MS), temporal evolution of paramagnetic rim lesions (PRL)-associated tissue damage, and its relationship to clinical disability, serum biomarkers, and treatment response remain incompletely understood.

Material and Methods

This multicentre study combined cross-sectional and longitudinal analyses of data from 182 MS cases (68% relapsing, 64% females; median EDSS 2.5 [range 0-8]). MRI-matched serum neurofilament light chain (sNfL) levels were measured and age corrected. PRL status was assessed on 3-tesla 3D-EPI-phase and lesion T1-times on MP2RAGE-maps. Lesions were classified as short-T1 (<1572ms) or long-T1 (≥1572ms). Longitudinal (~2.5y) lesion T1-time changes were analysed in a subset of pre/post anti-CD20 antibody treated (n=37) and untreated (n=37) cases.

Results

Lesion-age assessment in 134 lesions (72 PRL) showed that long-T1 PRL were older than short-T1 PRL (P = 0.015), with no differences in non-PRL. Adjusted analyses showed that short-T1 PRL volume correlated with higher sNfL z-scores (P = 0.026), whereas long-T1 PRL did not. Higher EDSS was associated with greater volume of long-T1 PRL (P = 0.003) but not short-T1 PRL. Pre/post treatment analyses showed significant treatment-related T1 decrease across different lesion subtypes, including short-T1 PRL (P < 0.01), whereas long-T1 PRL showed no detectable treatment effect (P = 0.8).

Conclusion

PRL show substantial heterogeneity in terms of MRI-measured lesional tissue damage, reflecting differences in the inflammatory/demyelinating and neurodegenerative processes across lesion development stages. Short-T1 PRL, likely representing younger lesions, are characterised by ongoing tissue damage and axonal degeneration, while long-T1 PRL correlate with established clinical disability. Our pre/post anti-CD20 analyses suggest that timely treatment of patients with short- T1 lesions might forestall future disability accrual in MS and that T1 changes in such lesions might serve as a predictive biomarker for this effect.

Funding

Intramural Research Program of NINDS, NIH; NINDS grants R01NS082347and R01NS082347; Dr. Miriam and Sheldon G. Adelson Medical Research Foundation; Fund for Scientific Research (FNRS); Sanofi Investigator Initiated Trial; Fondation Charcot Stichting Research Fund 2023 and 2025.

Keywords

Magnetic Resonance Imaging; Multiple Sclerosis; Advanced biomarkers; Paramagnetic Rim Lesions; Treatment Response; Lesion Aging

Research in Context

Evidence before this study

Paramagnetic rim lesions (PRL) are imaging markers of chronic active multiple sclerosis (MS) lesions and are associated with greater tissue damage and less favourable clinical outcomes. Previous histopathological and imaging studies suggest that quantitative T1 is sensitive to differences in lesional tissue integrity and may therefore help characterize the heterogeneity observed among PRL on magnetic resonance imaging (MRI). However, the origin of this heterogeneity is poorly understood. In particular, it is unclear whether differences in tissue integrity among PRL reflect distinct stages of lesion evolution and whether this heterogeneity is associated with clinical disability and treatment response.

Added value of this study

This study addressed three critical questions regarding the pathophysiological heterogeneity of PRL: (1) Is PRL heterogeneity linked to the temporal evolution of PRL? (2) Is PRL heterogeneity associated with serum neurofilament light chain (sNfL) levels? (3) Is PRL heterogeneity associated with differential treatment responses, and could this inform future treatment studies?

We found that PRL heterogeneity was associated with lesion age, potentially reflecting differences in inflammatory, demyelinating, and neurodegenerative processes across stages of lesion development. Short-T1 PRL, which showed less accumulated tissue damage and likely represented a younger lesion stage, were characterised by ongoing tissue damage and axonal degeneration, as indicated by their association with higher sNfL levels. By contrast, long-T1 PRL, which showed greater accumulated tissue damage, were associated with established clinical disability and accelerated brain ageing. Anti-CD20 pre-/post-treatment analyses further

suggested that T1 changes in short-T1 PRL might identify lesions responsive to treatment and could inform future treatment studies.

Implications of all the available evidence

Our findings suggest that PRL exhibit substantial heterogeneity in terms of lesional tissue damage, which is likely driven by differences in the inflammatory/demyelinating and neurodegenerative processes across the different stages of lesion development. Short-T1 PRL appear to represent lesions with ongoing tissue injury, whereas long-T1 PRL likely correspond to chronic lesions characterised by established tissue damage. Integrating T1-based lesion stratification with PRL assessment may improve patient stratification, by providing additional information about lesion stage and tissue integrity. The observed changes after anti-CD20 treatment further support the evaluation of short-T1 PRLs as candidate biomarkers of treatment-response in prospective studies.

Introduction

Focal smouldering inflammatory multiple sclerosis (MS) lesions, often seen as paramagnetic rim lesions (PRL), have been associated with disease severity and progression.(1–4) PRL are characterised by the presence of activated iron-laden microglia and macrophages at the lesion edge, which corresponds to a paramagnetic rim on susceptibility-sensitive magnetic resonance imaging (MRI).(5,6) PRL are considered a more destructive MS lesion type, highlighted by impaired lesional and perilesional tissue microstructure and larger lesion volumes.(7–10) However, recent studies suggest substantial T1-time heterogeneity within PRL, which has been shown to be associated with worse clinical outcomes, disability accumulation over time, and brain atrophy.(11,12) The origin of this heterogeneity remains unclear: whether it reflects the temporal evolution of PRL or other pathophysiological mechanisms is still debated.

Soluble biomarkers studies have shown that the presence of PRL is associated with elevated serum neurofilament light chain levels (sNfL), a biomarker of acute neuroaxonal damage.(13) Whether this biomarker can further elucidate the heterogeneity of PRL remains therefore an open question. Additionally, MS disease-modifying treatments (DMT) have shown at most a limited effect on PRL rim persistence, volume, and lesion-associated tissue damage.(14–16) This raises the question of whether PRL heterogeneity could serve as a stratification marker for treatment selection.

In this study, we address three critical questions regarding the pathophysiological heterogeneity of PRL: (1) Is PRL heterogeneity linked to the temporal evolution of PRL? (2) Is PRL heterogeneity associated with serum NfL? (3) Is PRL heterogeneity associated with differential treatment responses, and could this inform future treatment studies? By combining data from

two international centres using advanced MRI, clinical measures, and serum biomarkers, we investigate the importance of PRL heterogeneity in MS.

Materials and methods

Ethics

Clinical, imaging, and laboratory data were collected under the institutional review board-approved protocols from 2 academic research hospitals: Saint Luc University Hospitals (Brussels, Belgium) and the NIH Clinical Center (Bethesda, Maryland, USA). These protocols allowed exploratory analysis and pooling of collected data.

Study participants

Patient inclusion criteria for this retrospective analysis were: (1) age ≥ 18 years; (2) diagnosis of MS according to the current diagnostic criteria;(17) (3) availability of 3-tesla (3T) high-resolution segmented echo-planar imaging (EPI) T2*-weighted(18) and magnetization prepared 2 rapid gradient echo (MP2RAGE)(19) T1-weighted sequences in addition to standard clinical MRI (see Imaging Protocol); and (4) matched clinical-MRI assessment at baseline (Figure 1).

Clinical information, including Expanded Disability Status Scale (EDSS)(20) assessed by experienced MS clinicians, and laboratory (peripheral blood) samples were collected at the time of each MRI scan. Clinico-radiological relapse was defined as the presence of newly appearing or contrast-enhancing MRI lesions and/or new neurological symptoms in the 90 days preceding the baseline assessment. This was especially important for the sNfL analysis, where studies showed an elevation of sNfL after clinical relapses with gadolinium (gad)-lesions for

up to 3 months post relapse.(21–23) Treatment was categorized as follows: untreated, low efficacy drugs (glatiramer acetate, interferon), moderate efficacy drugs (dimethyl fumarate, sphingosine-1-phosphate modulators, teriflunomide, cladribine), high efficacy drugs (anti-CD20, natalizumab, alemtuzumab).

MRI acquisition and analysis

MRI studies were performed on two 3T MRI scanners: SIGNA (GE Health Care) at Saint Luc University Hospital and Siemens Skyra at NIH. The imaging protocol at both centres included: (1) submillimetre isotropic 3D T2*-weighted segmented EPI, providing both magnitude and phase images, for PRL detection; (2) 3D T2-weighted fluid-attenuated inversion recovery (FLAIR) for lesion segmentation; (3) 3D T1-weighted MP2RAGE providing T1 maps; and (4) post-gad T1-weighted to detect acutely inflamed lesions. For Saint-Luc patients, a 3D magnetization prepared rapid gradient echo (MPRAGE) sequence was acquired for brain volume assessment. Details on MRI protocols can be found in Supplementary Material and Methods.

Brain volumetrics were computed only for Saint-Luc patients, using FreeSurfer(24) on MPRAGE, and were normalized to total intracranial volume. Brain age was calculated using BrainageR, a widely used model in MS, as previously described,(25–27) and then normalized.(28) Based on the corrected predicted brain age, the brain-predicted age difference (brainPAD) was calculated, subtracting the chronological age from the brain-predicted age of each subject.(29) Positive brainPAD values indicated accelerated brain aging, while negative values suggest delayed brain aging.

PRL assessment

For each participant, the number of non-enhancing PRL was independently assessed at baseline on unwrapped filtered-phase images by two experienced raters (M.A. and P.M. for NIH data and A.S. and P.M. for Brussels data). In case of initial disagreement, a consensus was reached by the two raters in a separate session. PRL were assessed following the North American Imaging in Multiple Sclerosis (NAIMS) guidelines.(6) For lesion age and treatment analyses, PRL status was assessed on all available follow-up MRI.

Lesion volumetric and microstructural analysis

Brain lesions were segmented using FLAMeS,(30) and an in-house algorithm was used to separate individual lesions.(31) The resulting segmentation masks were then manually refined by an experienced rater (A.S.) to obtain an accurate lesion segmentation. In case of lesion confluency, lesions were split based on the T1 signal and rim topography on phase images. The final masks were restricted to the FLAIR-defined lesion boundaries and did not include surrounding periplaque tissue. Lesion volumes were calculated for each available MRI timepoint and log-normalised. MP2RAGE images were registered to the 3D-FLAIR images using ANTs,(32) and the lesion segmentations were subsequently rechecked. Mean lesional T1 times were calculated from T1 maps, and lesions were operationally categorized as short-T1 (mean T1 $<$ 1572ms) or long-T1 (mean T1 $\geq$ 1572ms) based on a previously described threshold,(11) consistent with prior histopathological classifications of T1 lesion subtypes (see also “Sensitivity Analysis: Histopathologically validated lesion classification” below).(33) Lesion compartment volumetrics (total short-T1 and long-T1 lesion volumes, PRL, short-T1 PRL and long-T1 PRL volumes) were calculated for every case.

Lesion-age analysis

Lesion-age analysis was available only for the Brussels cohort, for which longitudinal (including whenever available historical clinical) MRI scans were available. Each baseline analysed lesion was assessed for initial gad-enhancement on all previously available clinical and study MRI scans. Lesion age was then calculated as the time between first gad-enhancement and time of study MRI. For new lesions that appeared between two study MRIs, the lesion age was estimated as half the time interval between the two MRI scans, as previously described.(11) PRL status was assessed at each available MRI timepoint.

Serum Biomarkers

MRI-matched peripheral blood samples were collected for a subset of Brussels cases. sNfL levels were measured using the Atellica Immunoassay System (Siemens Healthineers Atellica® IM). All sNfL levels were z-score-corrected by age using a previously established reference normalization.(34)

Sensitivity Analysis: Histopathologically validated lesion classification

A previously established, histopathologically validated MRI classification(33) categorized lesions into three groups: short-T1 (predominantly remyelinated), mixed-T1 (partially de- and remyelinated), and long-T1 (demyelinated). Consistent with our prior findings, which showed a strong agreement between qualitative intensity-based and quantitative T1 relaxation time classifications,(11) we divided lesions into three categories according to the 25th and 75th

percentiles of the T1 distribution. This sensitivity (validation) analysis was performed for regression models with NfL, EDSS, and BrainPAD as outcomes.

Treatment Analysis

Treatment analyses were performed using three cohorts: (1) untreated throughout the entire observation period; (2) untreated at baseline and subsequently treated with anti-CD20 therapy (rituximab, ocrelizumab, or ofatumumab); and (3) already receiving anti-CD20 therapy at study inclusion. Cohorts 1-2 contributed to the "*pre-/post-treatment analysis,*" in which treatment initiation always occurred after the baseline MRI. For the "*post-treatment analysis,*" cohorts 1-3 were included, but only MRIs acquired under active treatment were considered, and the untreated baseline MRI of cohort 2 was excluded. For the *post-treatment analysis*, time under treatment at each MRI time point was calculated. All participants contributing untreated MRI time points had received no disease-modifying therapy for at least six months before the first untreated scan included in the analysis. Treatment effects were evaluated using mean T1 times and log-normalized lesion volumes relative to untreated lesions.

Statistical analysis

All statistical analyses were performed using R.(35) Demographic, clinical, and MRI differences were compared using univariable analysis including t-test, Mann-Whitney *U*-test, Standardized Mean Difference (SMD), or chi-squared test, as appropriate. Lesion-age analysis was performed using linear cross-sectional and longitudinal repeated-measures mixed models, accounting for random effects at the subject and lesion level when applicable. Serum biomarker, clinical score, and brain age associations were assessed using multivariable regression models, with covariates selected based on statistically significant associations

identified in univariable analyses. Because the different lesion-derived MRI measures (e.g., total PRL volume, long-T1 PRL volume, short-T1 PRL volume, and corresponding overall tissue measures) reflect overlapping aspects of lesion pathology, they were analysed in separate regression models. Continuous predictor variables were standardized (z-scored) prior to regression analysis to facilitate comparison of effect sizes across different measurement scales. Variable importance in random forest analyses was assessed using a conditional random forest model.(36–39) This approach accounts for collinearity among predictors by applying conditional permutation importance. Treatment effects were evaluated using linear mixed-effects models for repeated measures, accounting for random intercepts at the participant and lesion levels. Study centre and participant age were included as fixed effects to control for potential confounding. Tukey-adjusted post-hoc comparisons were used to compare outcome estimates between lesion types. A power analysis based on mixed-effects modelling was conducted by varying the number of included cases and lesions, as well as the slope difference between treatment arms, with 500 simulation runs per parameter combination. Given the exploratory nature of the analyses, no adjustment for multiple comparisons was applied, and p-values should be interpreted descriptively.

Role of Funders

This work was supported by the Intramural Program of NINDS of National Institutes of Health, by the National Institutes of Health (R01NS082347 and R01NS082347), by the Fund for Scientific Research (FRS, FNRS; grant #40008331), by a Sanofi Investigator Initiated Trial and by Fondation Charcot Stichting Research Fund 2023 and 2025. The funding sources had no role in study design, data collection, data analyses, interpretation, or writing of report.

Results

Of the total 182 participants (116 female, 64%) included in the study, 124 (68%) were labelled as relapsing remitting MS (RRMS) at baseline. Mean age was 44 (SD 13) years with median EDSS 2.5 [range 0 - 8]. Further clinical information can be found in Table 1.

PRL heterogeneity is associated with lesion age

Analysis of lesion age was restricted to a maximum of 4.5 years to avoid results driven by few datapoints with longer lesion age. Lesion age assessment was available for a subset of 134 lesions (72 PRL, 54%) in 35 cases. The median follow-up duration for this subset was 1 year (range 0 - 4.4). This lesion-age cohort did not differ from the full cohort in sex distribution or disease phenotype (all $P > 0.1$, all SMD<0.3) but was significantly younger overall (36 (SD 10) vs. 44 (SD 13) years; $P = 0.001$, SMD=0.7). Repeated measures linear mixed-effect modelling revealed an accelerated T1 increase in PRL after gad-resolution (β_{add_PRL}= 29.4ms/yr, 95% CI [13.9, 44.9], $P < 0.001$), in addition to the increase seen in non-PRL ($\beta_{non-PRL}$= 38.7ms/yr, 95% CI [27.5, 49.8], $P < 0.0001$; Figure 2A). No differences in lesion volume evolution over time were found between PRL and non-PRL ($P = 0.1$), although both lesion types showed a slight reduction of log-lesion volume over time. Full model coefficients are provided in *Supplementary Tables* 1 and 2.

Due to the limited sample size, separate cross-sectional mixed-effects models were fitted for PRL and non-PRL. In the non-PRL group, adjusted marginal means showed no significant difference in lesion age between short-T1 lesions (1.62 years, 95% CI [1.26,1.93]) and long-T1 lesions (2.05 years, 95% CI [1.38,2.71]), after accounting for patient age ($P = 0.20$, Figure 2B*).* Estimated marginal means adjusted for patient age showed that long-T1 PRL were older

(1.70 years, 95% CI [1.18,2.22]) than short-T1 PRL (1.43 years, 95% CI [0.93,1.93], $P = 0.015$, Figure 2C). Full model coefficients are provided in *Supplementary Tables* 3 and 4.

Soluble biomarkers and their association with PRL heterogeneity

In a subset of 125 cases, sNfL levels were measured and age-corrected (Figure 3). No significant differences in age, sex, or disease phenotype were observed between the full cohort and this NfL-cohort (all $P > 0.05$; all SMD<0.4). To assess the relative influence of known clinical and imaging variables, such as sex, relapse activity, and total volume of gad-enhancing lesions, treatment, and normalized brain volume on sNfL levels, we employed a random forest regression model. Additionally, total PRL volume, short-T1 PRL volume, and long-T1 PRL volume, as well as the total short-T1 and long-T1 lesion volume, were included as predictors in the analysis. Conditional variable importance scores from the random forest model were rescaled to set gad-enhancing lesion volume to 100%. On this relative scale, relapse activity (94%), total PRL volume (42%), and short-T1 PRL volume (37%) showed the greatest additional predictive contribution to sNfL levels.

Due to collinearity, five separate models were fitted for total PRL, long-T1 PRL, and short-T1 PRL volumes, as well as total short-T1 and long-T1 lesion volume, to ensure independent estimation of their associations with sNfL z-scores. Across all models, clinical or radiological relapse within the past 90 days was a consistent predictor of higher sNfL levels ($P \leq 0.02$), as was total gad-enhancing lesion volume ($P \leq 0.012$). Among the lesion measures of interest, higher total PRL volume (1SD = 741.4mm^3, $\beta = 0.15$, 95% CI [0.01, 0.30], $P = 0.032$) and higher total short-T1 PRL volume (1SD = 406.2mm^3, $\beta = 0.16$, 95% CI [0.02, 0.30], $P = 0.026$) were significantly associated with increased sNfL z-scores, whereas long-T1 PRL, short-T1 lesion volume, and long-T1 lesion volume were not ($P > 0.09$). Treatment status, sex, and T2

lesion load (T2LL) were not significant covariates in either model. In-depth model results can be found in *Supplementary Table* 5 and *Supplementary Fig* 2.

PRL heterogeneity is associated with clinical disability and accelerated brain aging

Random forest regression was used to assess associations between MRI measures and EDSS, including normalized brain volume, lesion compartment volumes, relapse activity, age, and treatment as predictors. Conditional variable importance scores were rescaled to set normalized brain volume to 100%. On this relative scale, age (73%), long-T1 PRL volume (32%), and T2LL (27%) showed the next-strongest contributions. Detailed random forest results are provided in the supplementary material. Due to collinearity between heterogeneity measures, these findings were validated in five distinct regression models, including age, sex, treatment, relapse activity, normalized brain volume, PRL, and general lesion heterogeneity measures as covariates. In all models, being treated with very high efficacy drugs ($P \leq 0.004$) and brain volume atrophy ($P \leq 0.001$) were associated with higher EDSS, with lesion-derived measures showing additional associations. Both PRL volume (1 SD = 1347mm^3, $\beta = 0.33$, 95% CI [0.05, 0.61], $P = 0.021$) and long-T1 PRL volume (1 SD = 695mm^3, $\beta = 0.40$, 95% CI [0.14, 0.67], $P = 0.003$) were associated with higher clinical disability, as was total long-T1 lesion volume (1 SD = 3963mm^3, $\beta = 0.46$, 95% CI [0.18, 0.74], $P = 0.002$), while no associations were found with short-T1 PRL ($P = 0.2$) or short-T1 lesion volume in general ($P = 0.08$). All regression results can be found in *Supplementary Table* 7 and *Supplementary Fig* 1.

Similarly, higher brainPAD (i.e., positive gap between brain predicted and chronological age) was associated with higher PRL volume (β = 0.47, 95% CI [0.09, 0.84], $P = 0.014$), long-T1 PRL volume (β = 0.41, 95% CI [0.12, 0.71], $P = 0.006$), and long-T1 lesion volume (β = 0.40,

95% CI [0.08, 0.71], $P = 0.013$). No significant associations were found for short-T1 PRL or short-T1 lesion volumes ($P = 0.12$). Across models, higher chronological age ($P \leq 0.026$) and treatment with very high-efficacy drugs ($P \leq 0.003$) were linked to higher brainPAD, whereas higher normalized brain volume was consistently associated with lower brainPAD ($P \leq 0.002$; *Supplementary Table* 8 and *Supplementary Fig* 3).

Sensitivity Analysis: Histopathologically validated lesion classification

A sensitivity analysis was performed to explore the associations between lesions groups, divided in three categories as previously proposed,(33) with sNfL, EDSS, and brainPAD. Lesions were classified according to mean T1 values as short-T1 (<1246 ms), mixed-T1 (≥1246 to <1570 ms), and long-T1 (≥1570 ms). When re-analysing the association between PRL heterogeneity and sNfL, mixed-T1 PRL emerged as the main correlate of elevated sNfL ($\beta = 0.26$, $P < 0.001$), exceeding the contribution of total gad-enhancing lesion volume and acute relapse. Other lesion categories, including short-T1 and long-T1 PRL, were not associated with higher sNfL (*Supplementary Table* 6). In the EDSS analyses, both mixed-T1 and long-T1 lesions, irrespective of PRL status, were associated with higher EDSS scores ($\beta = 0.40–0.45$, $P < 0.02$). Within PRL specifically, only long-T1 PRL were associated with higher EDSS ($\beta = 0.41$, $P = 0.003$; *Supplementary Table* 8). For BrainPAD, all lesion heterogeneity measures were associated with higher BrainPAD values ($\beta = 2.1–2.3$, $P < 0.002$), whereas among PRL, only long-T1 PRL were associated with higher BrainPAD ($\beta = 1.7$, $P = 0.008$; *Supplementary Table* 10).

PRL heterogeneity as a potential treatment target

In the *pre-/post-treatment analysis* (subset of 62 participants; 25 treated, 40%), lesion-level analyses were performed to compare anti-CD20-treated and untreated lesions. This treatment analysis cohort was similar to the full cohort in terms of sex and phenotype distribution but was slightly older (50 (SD 12) vs 44 (SD 13) years, P = 0.003, SMD=0.5). Participants underwent a baseline MRI before starting treatment. A total of 287 lesions were analysed (162 treated, 56%) for a median follow-up duration of 1.35 years (range 0.61 - 2.6 years). Of the 287 lesions included in the analysis, 104 were classified as PRL (37%), with 66 lesions being short-T1 (63%) and 38 long-T1 PRL (37%) at baseline. All PRL remained detectable throughout the observation period, with no evidence of rim disappearance or fading. Mean age for untreated cases was 50 (SD 13) years, while treated cases were slightly younger at 47 (SD 11) years (P = 0.042). For all treatment analyses, centre was included as a covariate to account for differences in MRI acquisitions, while patient age was included to account for its potential influence on longitudinal lesion changes.

Repeated-measures mixed models of all lesions, independent of lesion type, showed a significant increase of T1 over time in lesions from untreated participants ($\beta_{untreated}$ = 25.1ms/y, 95% CI [11.76, 38.4], P < 0.001*)*, while lesions from treated participants showed a significant decrease of T1 ($\beta_{add\_treated}$ = -62.5ms/y, 95% CI [-80.1, -44.9], P < 0.0001). Baseline T1 was higher in lesions from treated participants compared to lesions from untreated participants ($\beta_{add\_treated}$ = 133.6ms, 95% CI [32.6, 234.7], P = 0.01, *Supplementary Table* 11*)*. In a separate mixed-effects model examining longitudinal lesion volume, lesions from untreated participants showed a slight increase of the average log-lesion volume ($\beta_{untreated}$ = 0.08, 95% CI [0.01, 0.15], P = 0.029*)*, corresponding to an 8% increase in lesion volume (95% CI: 1-16%). No significant

treatment-associated effect was observed on the average log-lesion volume over time ($\beta_{add\_treated}$ = -0.08, 95% CI [-0.17, 0.01], P = 0.1; *Supplementary Table* 12).

In a mixed-effects model adjusting for centre, age, lesion type, T1-status, and treatment, we observed a significant four-way interaction between follow-up time, treatment, lesion type, and T1-status ($F(1, 244)=4.84$, P = 0.029), indicating that longitudinal T1 changes were associated with both lesion subtype (PRL / T1 status) and treatment. In non-PRL, lesions from untreated participants showed an increase in T1 over time ($\beta_{short\text{-}T1\ non\text{-}PRL}$ = 22.3ms/y, 95% CI [7.5, 37.0]; $\beta_{long\text{-}T1\ non\text{-}PRL}$ = 57.6 ms/y, 95% CI [11.0, 104.2]), whereas lesions from treated participants showed an average decrease in T1 ($\beta_{short\text{-}T1\ non\text{-}PRL}$ = –39.9 ms/y, 95% CI [–55.8, –24.0]; $\beta_{long\text{-}T1\ non\text{-}PRL}$ = –58 ms/y, 95% CI [–126.1, 10.2]; Figure 4 B and D).

In PRL, short-T1 PRL showed a similar pattern with an average T1 decrease in lesions from treated participants (untreated: $\beta_{short\text{-}T1\ PRL}$ = 30.8 ms/y, 95% CI [–22.2, 83.7]; treated: $\beta_{short\text{-}T1\ PRL}$ = –43.9 ms/y, 95% CI [–62.7, –25.1]). However, long-T1 PRL lesions showed minimal T1 change regardless of their treatment status (untreated: $\beta_{long\text{-}T1\ PRL}$ = –1.9 ms/y, 95% CI [–59.5, 55.7]; treated: $\beta_{long\text{-}T1\ PRL}$ = 6.36 ms/y, 95% CI [–28.2, 40.9]; Figure 4C and E; *Supplementary Table* 13).

Post-hoc simple-slope contrasts comparison recapitulated significant treatment effects in all lesion categories except for long-T1 PRL. Significant differences between treated and untreated T1 trajectories were observed in short-T1 non-PRL ($\Delta\beta$ = –62.2 ms/y, 95% CI [40.5, 83.9], $P < 0.0001$), short-T1 PRL ($\Delta\beta$ = –74.7 ms/y, 95% CI [18.5, 130.8], P = 0.0094), and long-T1 non-PRL ($\Delta\beta$ = –115.6 ms/y, 95% CI [33.0, 198.1], P = 0.009), while no significant effect was detected in long-T1 PRL ($\Delta\beta$ = +8.28 ms/y, 95% CI [-75.5, 58.9], P = 0.8; *Supplementary Table* 14).

A second mixed-effects model evaluating treatment effect on the log-transformed lesion volume (using the same predictors) revealed no significant four-way interaction ($P = 0.3$) and no significant treatment-related interactions at lower levels, indicating that treatment effects on lesion volume did not vary by PRL or T1 status (*Supplementary Tables* 15 and 16).

In the *post-treatment analysis* (including all cases with at least 1 post-treatment time point; see "Treatment analysis" section of the methods), a total of 74 cases were included (37 treated, 50%), with a total of 333 lesions (120 PRL, 35.9%). Treated cases were younger than untreated ones (mean 44 (SD 11) vs 50 (SD 13) years, respectively; $P = 0.008$). Median treatment duration was 1.5 years (range 0.4 - 3.6 years). Results of these analyses were in line with those of the *pre-/post-treatment analysis* showing a reduction of average lesion T1 times in lesions from treated vs untreated patients ($\beta_{add\_treated}$ = -77.52ms/y, 95% CI [-96.7, -58.4], $P < 0.001$), as well as in PRL from treated vs untreated participants ($\beta_{add\_treated}$ = -79.12ms/y, 95% CI [-114.0, -44.3], $P < 0.001$). Finally, and in line with the *pre-/post-treatment analysis*, no significant treatment effect on PRL volume was observed. Full model coefficients are provided in *Supplementary Tables* 19 - 22.

Treatment Power Analysis

To complement the treatment analysis (*pre-/post-treatment dataset*), we performed a post-hoc power analysis varying the number of included cases, lesions, and slope difference between treatment arms (*Supplementary Tables* 11 and 18). Across the tested parameter ranges, statistical power remained consistently high. Consistent with our treatment findings, simulations indicated that a sample of 60 cases and approximately 200 lesions would provide power of 85% to detect a slope difference of at least 30ms between untreated and treated lesions, both across all lesions and within PRL. These results suggest that similar study designs

would be well powered to detect differences of comparable magnitude. Detailed results of this analysis are provided in *Supplementary Figs* 4 and 5 for reference**.**

Discussion

Chronic active MS lesions, identified as PRL on in vivo MRI, are being increasingly recognized as key contributors to the diagnostic and prognostic assessment.(17) Yet, a substantial heterogeneity exists in PRL-associated tissue damage,(7,11,12,33,40) which may influence their clinical applicability.

In this study, we demonstrate that PRL exhibit substantial heterogeneity in terms of lesional tissue damage, which is likely driven by differences in the inflammatory/demyelinating and neurodegenerative processes across the different stages of lesion development (Figure 5). Specifically, short-T1 PRL likely represent an earlier stage of lesion development, characterised by younger lesion age and ongoing neuroaxonal damage, as reflected by higher sNfL levels. In contrast, long-T1 PRL are characterised by already advanced tissue damage and strongly correlate with established clinical disability and brain aging. These associations suggest that short-T1 PRL (and mixed-T1 PRL in our sensitivity analyses) could represent an active, transitional stage of PRL development, whereas long-T1 PRL may reflect chronic, potentially irreversible, tissue damage. These findings are consistent with prior imaging and histopathological studies demonstrating that increasing T1 values reflect greater structural tissue damage.(33) Our preliminary *treatment analyses* suggest that timely treatment of patients with short-T1 PRL, for example with CNS-penetrant immunomodulatory therapies, might attenuate tissue damage accrual and thereby forestall future or possibly even reverse disability accumulation in MS.

Our *lesion-age analyses* further support this interpretation. Indeed, our findings suggest that PRL undergo accelerated tissue damage accumulation over the ~4-year observational period. This dynamic was further supported by the younger lesion age of short-T1 PRL vs long-T1 PRL, a lesion-age gap that could not be observed in non-PRL. This apparent discrepancy between PRL and non-PRL might be explained by differences in their evolutional trajectories. Indeed, short-T1 non-PRL lesions are likely to stay short-T1 over time, while PRL seem to follow a more dynamic course characterised by faster tissue destruction and progression from short-T1 to long-T1 stages. Consistently, short-T1 PRL cluster at younger lesion ages, whereas short-T1 non-PRL are distributed across a wider range of lesion ages. Of note, lesion-volume evolution did not significantly differ between PRL and non-PRL, indicating that these T1 changes were not accompanied by detectable differences in lesion size.

In line with previous results,(13) PRL showed associations with elevated sNfL levels, even after adjusting for recent clinical or radiological relapse activity. Notably, short-T1 PRL contributed significantly to this association, whereas long-T1 PRL did not. Interestingly, short-T1 lesions in general were not associated with sNfL, highlighting the significant role of chronic active (vs chronic inactive) lesions in explaining neuroaxonal damage in MS. These findings were confirmed in our sensitivity analysis where only mixed-T1 (but not short-T1 or long-T1) PRL, representing partially de-myelinated lesions,(33) were associated with elevated sNfL. Considering that acute inflammation in MS leads to an active and relatively rapid increase in sNfL levels, the observed association with short-T1 PRL highlights that this lesion subtype represents an active stage of ongoing tissue injury and accumulating tissue damage. This aligns with our *lesion-age analysis*, showing that tissue damage within PRL progressively increases over time.(41,42) The absence of an association between long-T1 PRL and sNfL supports the notion that, once PRL transition into a “more stable” chronic active stage (after about two years), the chronic-active-inflammation-driven neuroaxonal damage substantially attenuates.

As previously reported,(11,12) long-T1 PRL, potentially representing an older lesion stage, were strongly associated with clinical disability and accelerated brain aging.(27) In contrast with our sNfL findings — where short-T1 PRL were the main contributors — clinical disability and brain aging appeared to be mainly associated with long-T1 lesions. This is not unexpected, as "black holes" with long T1 times are known to be associated with worse clinical disability.(12,43) These results further emphasize the clinical relevance of lesion-level heterogeneity. Notably, compared to long-T1 lesions overall (i.e., irrespective of PRL status), a smaller long-T1 PRL volume (average long-T1 PRL volume/case) was sufficient to show an effect on EDSS.

Finally, our exploratory treatment analyses showed a potential effect of anti-CD20 drugs on mean PRL T1 times. Consistent with previous studies,(14,44) treatment did not measurably affect lesion volume or rim visibility; however, a differential effect on T1 time trajectories was evident. Across non-PRL, independently of their T1 status, lesions from untreated participants showed a clear reduction in T1 over time, whereas T1 increased in lesions from untreated participants. A similar treatment-related decline was also present in short-T1, likely younger, PRL. In contrast, long-T1 PRL showed virtually no change in T1 times, with no detectable treatment-associated effect, suggesting that more advanced tissue damage within PRL may be refractory to therapeutic modulation with peripherally acting anti-CD20 antibodies. A possible explanation for these differences within PRL might be the degree of compartmentalization of the inflammatory response (likely higher in long-T1 PRL)(45) and to different cellular profile of the rim.(14,46,47) Given that PRL are strongly associated with neuroaxonal damage and future disability progression,(3,14,48,49) attenuation of tissue damage accrual within PRL, especially short-T1 PRL, may be of particular clinical relevance. In light of previous reports showing limited treatment effects on lesion measures (especially lesion volume),(14,15,44,50) assessing treatment responses through baseline measures of lesion heterogeneity may provide

greater sensitivity. Our *power analyses* suggest that including about 60 cases would be sufficient to detect a treatment effect on T1 times within PRL (even in the case of a more modest 30ms slope difference between treated/untreated lesions).

A major limitation of this study is the relatively small sample size of our *lesion-age analysis* and the resulting inability to adjust for potential confounding factors, particularly treatment. However, the acquisition of longitudinal lesion-level data required for lesion age estimation remains highly challenging, and such datasets are currently scarce. Given the observed anti-CD20-related effects in short-T1 lesions, we cannot exclude the possibility that the longitudinal evolution of these lesions may also be affected by other treatments. Collecting such longitudinal data, especially from entirely untreated patients, remains challenging, as individuals with PRL are generally more likely to receive second-line therapies.(51) Furthermore, our *lesion-age analysis* is currently limited to a follow-up period of 4.5 years, which does not capture the full life cycle of PRL, estimated to last a median of 7-10 years.(10,47,52) While our data support this developmental interpretation, it is important to acknowledge that lesion age cannot always be determined with perfect precision. For enhancing lesions, age is known from the time of first gadolinium enhancement, whereas lesions appearing between two imaging sessions are assigned an estimated onset at the midpoint between scans. As such, lesion age carries a certain degree of temporal uncertainty, particularly for intervally developing lesions. PRL detectability is also influenced by acquisition parameters of susceptibility-sensitive imaging, including echo time, spatial resolution, and field strength, which may lead to underestimation of rim prevalence, particularly in older or smaller lesions. Furthermore, slowly expanding lesion status was not available in this study and could therefore not be considered in the interpretation of lesion-volume trajectories. The cross-sectional design of our *fluid biomarker* and *disability analyses* also restricts causal interpretation and limits insight into the longitudinal effects of short-T1

and long-T1 PRL on disability accrual. Finally, our *treatment analysis* was exploratory and restricted to a 2.5-year observation period. As such, it remains unclear whether the observed attenuation of tissue damage accrual — particularly in short-T1 PRL — translates into long-term reductions in disability progression. Furthermore, these findings may not generalize to less active MS populations, such as patients with longstanding MS. In addition, subgroup sample sizes, most notably for long-T1 non-PRL lesions, were limited, and findings in these strata should therefore be interpreted with caution. Lastly, although quantitative T1 has been associated with myelination levels in histopathological studies,(33) no additional myelin-sensitive imaging was available in the present cohort. Therefore, short-, mixed- and long-T1 lesions should be interpreted as lesions reflecting differences in tissue integrity rather than definitive myelination states.

Future longitudinal studies combining advanced quantitative MRI, histopathological validation, and standardized treatment documentation will be essential to clarify the temporal dynamics of PRL subtypes, their associations with future disability progression, and their responsiveness to therapy.

In conclusion, PRL show distinct heterogeneity in terms of their quantitative T1 measures, potentially reflecting different stages in lesion development. While long-T1 PRL appear to represent a more advanced stage of chronic inflammatory activity with accumulated tissue damage — associated with clinical disability and largely unresponsive to treatment — short-T1 PRL may be of particular interest for future studies on disability progression and therapeutic responsiveness.

Author's contribution

AS: Data curation, Conceptualisation, Methodology, Formal analysis, Investigation, Writing - Original Draft, Validation, Visualisation

CVD: Data Curation, Visualisation, Conceptualisation, Writing - Review & Editing

SB: Data Curation, Visualisation, Conceptualisation, Writing - Review & Editing

MD: Data Curation, Visualisation, Conceptualisation, Writing - Review & Editing

JLB: Data Curation, Visualisation, Conceptualisation, Writing - Review & Editing

EVD: Data Curation, Visualisation, Conceptualisation, Writing - Review & Editing

CB: Data Curation, Writing – Review & Editing, Conceptualisation, Investigation

VvP: Data Curation, Writing – Review & Editing, Conceptualisation, Investigation

MIG: Data Curation, Writing – Review & Editing, Conceptualisation, Investigation

MA: Writing - Original Draft, Conceptualisation, Data Curation, Supervision, Investigation, Resources, Project administration

DSR: Writing - Original Draft, Conceptualisation, Data Curation, Supervision, Investigation, Resources, Project administration

PM: Writing - Original Draft, Conceptualisation, Data Curation, Supervision, Investigation, Resources, Project administration

Declaration of Interests

Anna Stölting: has the financial support of the Fédération Wallonie Bruxelles – FRIA du Fonds de la Recherche Scientifique – FNRS.

Colin Vanden Bulcke: nothing to disclose.

Serena Borrelli: is supported by the Funds Claire Fauconnier, Ginette Krykstein & José and Marie Philippart-Hoffelt, managed by the King Baudouin Foundation. She has received unrelated research funding from Roche, Sanofi, and Brugmann Foundation.

Matthieu Deltombe: nothing to disclose.

Jean-Louis Bayart: nothing to disclose.

Eline Van Doninck: is supported by FWO-TBM (project MACSiMiSE-BRAIN—T001121N)

Céline Bugli: nothing to disclose.

Vincent van Pesch: has received travel grants from Merck Healthcare KGaA (Darmstadt, Germany), Biogen, Sanofi, Bristol Meyer Squibb, Almirall and Roche. His institution has received research grants and consultancy fees from Roche, Biogen, Sanofi, Merck Healthcare KGaA (Darmstadt, Germany), Bristol Meyer Squibb, Janssen, Almirall, Novartis Pharma, and Alexion. María I. Gaitán: nothing to disclose.

Martina Absinta: received research support from the European Research Council, National MS Society, Conrad N Hilton Foundation, International Progressive MS Alliance, Cariplo Foundation, FRRB Early Career Award, and FISM - Fondazione Italiana Sclerosi Multipla co-financed with the '5 per mille' public funding. MA also received consultancy and/or speaker honoraria from Sanofi, GSK, Biogen, Roche and Immunic Therapeutics.

Daniel S. Reich: has received research funding from Abata and Sanofi.

Pietro Maggi: is supported by the Fondation Charcot Stichting Research Fund 2023 and 2025, the Fund for Scientific Research (F.R.S, FNRS; grant #40008331), Cliniques universitaires Saint-Luc "Fonds de Recherche Clinique", Biogen and Sanofi. He has received consulting honoraria from Sanofi, Biogen, Merck and Novartis.

This research was partially supported by Sanofi.

This research was supported in part by the Intramural Research Program of the National Institutes of Health (NIH). The contributions of the NIH authors are considered Works of the United States Government. The findings and conclusions presented in this paper are those of the authors and do not necessarily reflect the views of the NIH or the U.S. Department of Health and Human Services.

Acknowledgements

The authors thank the study participants; the neuroimmunology clinics of cliniques universitaires Saint-Luc (CUSL, Brussels, Belgium) and NINDS (NIH Clinical Center, Bethesda, Maryland, USA) for recruiting and evaluating the patients and for coordinating the scans; Thierry Duprez, Sébastien de Laever (CUSL), Laurence Dricot (Université catholique de Louvain), Gaëtan Duchenes (CUSL), Océane Perdaens (CUSL) and Julie Poujol (GE Healthcare) for assistance with 3T MRI scan acquisition and analysis in Brussels.

Data Sharing Statement

Data will be shared upon establishment of a data-sharing agreement with formal approval from the local ethics committee.

References

1. Giovannoni G, Popescu V, Wuerfel J, Hellwig K, Iacobaeus E, Jensen MB, et al. Smouldering multiple sclerosis: the "real MS." Ther Adv Neurol Disord. 2022;15:17562864211066751. doi:10.1177/17562864211066751 PubMed PMID: 35096143; PubMed Central PMCID: PMC8793117.

2. Müller J, Cagol A, Lorscheider J, Tsagkas C, Benkert P, Yaldizli Ö, et al. Harmonizing Definitions for Progression Independent of Relapse Activity in Multiple Sclerosis: A Systematic Review. JAMA Neurology. 2023 Nov 1;80(11):1232–45. doi:10.1001/jamaneurol.2023.3331

3. Absinta M, Sati P, Masuzzo F, Nair G, Sethi V, Kolb H, et al. Association of Chronic Active Multiple Sclerosis Lesions With Disability In Vivo. JAMA Neurol. 2019 Dec 1;76(12):1474–83. doi:10.1001/jamaneurol.2019.2399 PubMed PMID: 31403674; PubMed Central PMCID: PMC6692692.

4. Cagol A, Benkert P, Melie-Garcia L, Schaedelin SA, Leber S, Tsagkas C, et al. Association of Spinal Cord Atrophy and Brain Paramagnetic Rim Lesions With Progression Independent of Relapse Activity in People With MS. Neurology. 2024 Jan 9;102(1):e207768. doi:10.1212/WNL.0000000000207768

5. Absinta M, Sati P, Fechner A, Schindler MK, Nair G, Reich DS. Identification of Chronic Active Multiple Sclerosis Lesions on 3T MRI. American Journal of Neuroradiology. 2018 Jul 1;39(7):1233–8. doi:10.3174/ajnr.A5660 PubMed PMID: 29724768.

6. Bagnato F, Sati P, Hemond CC, Elliott C, Gauthier SA, Harrison DM, et al. Imaging chronic active lesions in multiple sclerosis: a consensus statement. Brain. 2024 Jan 16;awae013. doi:10.1093/brain/awae013

7. Vanden Bulcke C, Stölting A, Maric D, Macq B, Absinta M, Maggi P. Comparative overview of multi-shell diffusion MRI models to characterize the microstructure of multiple sclerosis lesions and periplaques. NeuroImage: Clinical. 2024 Mar 1;42:103593. doi:10.1016/j.nicl.2024.103593

8. Absinta M, Sati P, Schindler M, Leibovitch EC, Ohayon J, Wu T, et al. Persistent 7-tesla phase rim predicts poor outcome in new multiple sclerosis patient lesions. J Clin Invest. 2016 Jul 1;126(7):2597–609. doi:10.1172/JCI86198 PubMed PMID: 27270171; PubMed Central PMCID: PMC4922708.

9. Dal-Bianco A, Grabner G, Kronnerwetter C, Weber M, Höftberger R, Berger T, et al. Slow expansion of multiple sclerosis iron rim lesions: pathology and 7 T magnetic resonance imaging. Acta Neuropathol. 2017 Jan;133(1):25–42. doi:10.1007/s00401-016-1636-z

10. Dal-Bianco A, Grabner G, Kronnerwetter C, Weber M, Kornek B, Kasprian G, et al. Long-term evolution of multiple sclerosis iron rim lesions in 7 T MRI. Brain. 2021 Mar 1;144(3):833–47. doi:10.1093/brain/awaa436

11. Stölting A, Vanden Bulcke C, Borrelli S, Bugli C, Du Pasquier R, van Pesch V, et al. Clinical relevance of paramagnetic rim lesion heterogeneity in multiple sclerosis. Annals of Clinical and Translational Neurology. 2024;11(12):3137–51. doi:10.1002/acn3.52220

12. Shi Z, Wang H, Yan Z, Tang Y, Moccia M, Nie L, et al. T1-based stratification of paramagnetic rim lesions in multiple sclerosis: Evidence of microstructural heterogeneity and clinical implications. Mult Scler. 2025 Nov 10;13524585251389809. doi:10.1177/13524585251389809

13. Maggi P, Kuhle J, Schädelin S, Meer F van der, Weigel M, Galbusera R, et al. Chronic White Matter Inflammation and Serum Neurofilament Levels in Multiple Sclerosis. Neurology. 2021 Aug 10;97(6):e543–53. doi:10.1212/WNL.0000000000012326 PubMed PMID: 34088875.

14. Maggi P, Bulcke CV, Pedrini E, Bugli C, Sellimi A, Wynen M, et al. B cell depletion therapy does not resolve chronic active multiple sclerosis lesions. eBioMedicine. 2023 Aug;94:104701. doi:10.1016/j.ebiom.2023.104701

15. Zinger N, Ponath G, Sweeney E, Nguyen TD, Lo CH, Diaz I, et al. Dimethyl Fumarate Reduces Inflammation in Chronic Active Multiple Sclerosis Lesions. Neurol Neuroimmunol Neuroinflamm. 2022 Jan 19;9(2):e1138. doi:10.1212/NXI.0000000000001138 PubMed PMID: 35046083; PubMed Central PMCID: PMC8771666.

16. Reeves JA, Bartnik A, Mohebbi M, Ramanathan M, Bergsland N, Jakimovski D, et al. Determinants of long-term paramagnetic rim lesion evolution in people with multiple sclerosis. Annals of Clinical and Translational Neurology. 2025;12(2):267–79. doi:10.1002/acn3.52253

17. Montalban X, Lebrun-Frénay C, Oh J, Arrambide G, Moccia M, Amato MP, et al. Diagnosis of multiple sclerosis: 2024 revisions of the McDonald criteria. The Lancet Neurology. 2025 Oct 1;24(10):850–65. doi:10.1016/S1474-4422(25)00270-4

18. Sati P, Thomasson D, Li N, Pham D, Biassou N, Reich D, et al. Rapid, high-resolution, whole-brain, susceptibility-based MRI of multiple sclerosis. Multiple sclerosis (Houndmills, Basingstoke, England). 2014 Mar 17;20. doi:10.1177/1352458514525868

19. Marques JP, Kober T, Krueger G, van der Zwaag W, Van de Moortele PF, Gruetter R. MP2RAGE, a self bias-field corrected sequence for improved segmentation and T1-mapping at high field. Neuroimage. 2010 Jan 15;49(2):1271–81. doi:10.1016/j.neuroimage.2009.10.002 PubMed PMID: 19819338.

20. Kurtzke JF. Rating neurologic impairment in multiple sclerosis: an expanded disability status scale (EDSS). Neurology. 1983 Nov;33(11):1444–52. doi:10.1212/wnl.33.11.1444 PubMed PMID: 6685237.

21. Bar-Or A, Montalban X, Hu X, Kropshofer H, Kukkaro P, Coello N, et al. Serum Neurofilament Light Trajectories and Their Relation to Subclinical Radiological Disease Activity in Relapsing Multiple Sclerosis Patients in the APLIOS Trial. Neurol Ther. 2023 Feb;12(1):303–17. doi:10.1007/s40120-022-00427-8 PubMed PMID: 36534274; PubMed Central PMCID: PMC9837345.

22. Rosso M, Gonzalez CT, Healy BC, Saxena S, Paul A, Bjornevik K, et al. Temporal association of sNfL and gad-enhancing lesions in multiple sclerosis. Ann Clin Transl Neurol. 2020 Jun;7(6):945–55. doi:10.1002/acn3.51060 PubMed PMID: 32452160; PubMed Central PMCID: PMC7318095.

23. Chitnis T, Magliozzi R, Abdelhak A, Kuhle J, Leppert D, Bielekova B. Blood and CSF biomarkers for multiple sclerosis: emerging clinical applications. The Lancet Neurology. 2025 Sep 24;0(0). doi:10.1016/S1474-4422(25)00249-2 PubMed PMID: 41015047.

24. Fischl B, Salat DH, Busa E, Albert M, Dieterich M, Haselgrove C, et al. Whole brain segmentation: automated labeling of neuroanatomical structures in the human brain. Neuron. 2002 Jan 31;33(3):341–55. doi:10.1016/s0896-6273(02)00569-x PubMed PMID: 11832223.

25. Karatzoglou A, Smola A, Hornik K, Zeileis A. kernlab-an S4 package for kernel methods in R. Journal of statistical software. 2004;11(1):1–20.

26. Cole JH, Poudel RPK, Tsagkrasoulis D, Caan MWA, Steves C, Spector TD, et al. Predicting brain age with deep learning from raw imaging data results in a reliable and heritable biomarker. Neuroimage. 2017 Dec;163:115–24. doi:10.1016/j.neuroimage.2017.07.059 PubMed PMID: 28765056.

27. Fagiani F, Pedrini E, Martire MS, Gastoldi G, Vanden Bulcke C, Lin JP, et al. Spatially-restricted inflammation-induced senescent-like glia in multiple sclerosis and patient-derived organoids. Nat Commun. 2025 Sep 26;16(1):8477. doi:10.1038/s41467-025-63371-9

28. Cole JH, Raffel J, Friede T, Eshaghi A, Brownlee WJ, Chard D, et al. Longitudinal Assessment of Multiple Sclerosis with the Brain-Age Paradigm. Annals of Neurology. 2020;88(1):93–105. doi:10.1002/ana.25746

29. Borrelli S, Guisset F, Vanden Bulcke C, Stölting A, Bugli C, Lolli V, et al. Enlarged perivascular spaces are associated with brain microangiopathy and aging in multiple sclerosis. Mult Scler. 2024 Jul;30(8):983–93. doi:10.1177/13524585241256881 PubMed PMID: 38850029.

30. Dereskewicz E, Rosa FL, Silva J dos S, Sizer E, Kohli A, Wynen M, et al. FLAMeS: A Robust Deep Learning Model for Automated Multiple Sclerosis Lesion Segmentation [Internet]. medRxiv; 2025 [cited 2025 Nov 4]. p. 2025.05.19.25327707. Available from: https://www.medrxiv.org/content/10.1101/2025.05.19.25327707v1 doi:10.1101/2025.05.19.25327707

31. Vanden Bulcke C, Stölting A, Borrelli S, Macq B, Cuadra MB, Absinta M, et al. Do slowly expanding lesions correspond to chronic active multiple sclerosis lesions? An integrated imaging analysis study [Internet]. medRxiv; 2025 [cited 2026 Jan 15]. p. 2025.12.03.25341192. Available from: https://www.medrxiv.org/content/10.64898/2025.12.03.25341192v1 doi:10.64898/2025.12.03.25341192

32. Tustison NJ, Cook PA, Holbrook AJ, Johnson HJ, Muschelli J, Devenyi GA, et al. The ANTsX ecosystem for quantitative biological and medical imaging. Sci Rep. 2021 Apr 27;11(1):9068. doi:10.1038/s41598-021-87564-6

33. Kolb H, Absinta M, Beck ES, Ha SK, Song Y, Norato G, et al. 7T MRI Differentiates Remyelinated from Demyelinated Multiple Sclerosis Lesions. Ann Neurol. 2021 Oct;90(4):612–26. doi:10.1002/ana.26194 PubMed PMID: 34390015; PubMed Central PMCID: PMC9291186.

34. Fitzgerald KC, Sotirchos ES, Smith MD, Lord HN, DuVal A, Mowry EM, et al. Contributors to serum NfL levels in people without neurologic disease. Ann Neurol. 2022 Oct;92(4):688–98. doi:10.1002/ana.26446 PubMed PMID: 35730070; PubMed Central PMCID: PMC9489658.

35. R Core Team. R: A Language and Environment for Statistical Computing [R] [Internet]. Vienna, Austria: R Foundation for Statistical Computing; 2023. Available from: https://www.R-project.org/

36. Hothorn T, Hornik K, Zeileis A. Unbiased Recursive Partitioning: A Conditional Inference Framework. Journal of Computational and Graphical Statistics. 2006 Sep 1;15(3):651–74. doi:10.1198/106186006X133933

37. Zeileis A, Hothorn T, Hornik K. Model-Based Recursive Partitioning. Journal of Computational and Graphical Statistics. 2008 Jun 1;17(2):492–514. doi:10.1198/106186008X319331

38. Hothorn T, Zeileis A. partykit: A Modular Toolkit for Recursive Partytioning in R. Journal of Machine Learning Research. 2015;16(118):3905–9.

39. Liaw A, Wiener M. Classification and Regression by randomForest [Internet]. 2002. Available from: https://CRAN.R-project.org/doc/Rnews/

40. Rahmanzadeh R, Galbusera R, Lu PJ, Bahn E, Weigel M, Barakovic M, et al. A New Advanced MRI Biomarker for Remyelinated Lesions in Multiple Sclerosis. Annals of Neurology. 2022;92(3):486–502. doi:10.1002/ana.26441

41. Rosso M, Gonzalez CT, Healy BC, Saxena S, Paul A, Bjornevik K, et al. Temporal association of sNfL and gad-enhancing lesions in multiple sclerosis. Ann Clin Transl Neurol. 2020 May 25;7(6):945–55. doi:10.1002/acn3.51060 PubMed PMID: 32452160; PubMed Central PMCID: PMC7318095.

42. Meier S, Willemse EAJ, Schaedelin S, Oechtering J, Lorscheider J, Melie-Garcia L, et al. Serum Glial Fibrillary Acidic Protein Compared With Neurofilament Light Chain as a Biomarker for Disease Progression in Multiple Sclerosis. JAMA Neurol. 2023 Feb 6;80(3):287–97. doi:10.1001/jamaneurol.2022.5250 PubMed PMID: 36745446; PubMed Central PMCID: PMC10011932.

43. Rocca MA, Comi G, Filippi M. The Role of T1-Weighted Derived Measures of Neurodegeneration for Assessing Disability Progression in Multiple Sclerosis. Front Neurol. 2017 Sep 4;8. doi:10.3389/fneur.2017.00433

44. Amin M, Nakamura K, Thoomukuntla B, Carlson AK, Planchon SM, Moore S, et al. Paramagnetic rim lesions on 7T MRI after autologous hematopoietic cell transplantation. Mult Scler. 2026 Mar 13;13524585261429371. doi:10.1177/13524585261429371

45. Hemond CC, Baek J, Ionete C, Reich DS. Paramagnetic rim lesions are associated with pathogenic CSF profiles and worse clinical status in multiple sclerosis: a retrospective cross-sectional study. Mult Scler. 2022 Nov;28(13):2046–56. doi:10.1177/13524585221102921 PubMed PMID: 35748669; PubMed Central PMCID: PMC9588517.

46. Kuhlmann T, Ludwin S, Prat A, Antel J, Brück W, Lassmann H. An updated histological classification system for multiple sclerosis lesions. Acta Neuropathol. 2017 Jan 1;133(1):13–24. doi:10.1007/s00401-016-1653-y

47. Absinta M, Maric D, Gharagozloo M, Garton T, Smith MD, Jin J, et al. A lymphocyte–microglia–astrocyte axis in chronic active multiple sclerosis. Nature. 2021 Sep;597(7878):7878. doi:10.1038/s41586-021-03892-7

48. Borrelli S, Martire MS, Stölting A, Vanden Bulcke C, Pedrini E, Guisset F, et al. Central Vein Sign, Cortical Lesions, and Paramagnetic Rim Lesions for the Diagnostic and Prognostic Workup of Multiple Sclerosis. Neurology Neuroimmunology & Neuroinflammation. 2024 Jul;11(4):e200253. doi:10.1212/NXI.0000000000200253

49. Toru Asahina A, Lu J, Chugh P, Sharma S, Sharma P, Tan S, et al. Prognostic significance of paramagnetic rim lesions in multiple sclerosis: A systematic review. Journal of Clinical Neuroscience. 2024 Nov 1;129:110810. doi:10.1016/j.jocn.2024.110810

50. Elliott C, Belachew S, Wolinsky JS, Hauser SL, Kappos L, Barkhof F, et al. Chronic white matter lesion activity predicts clinical progression in primary progressive multiple sclerosis. Brain. 2019 Sep 1;142(9):2787–99. doi:10.1093/brain/awz212 PubMed PMID: 31497864; PubMed Central PMCID: PMC6736181.

51. Maggi P, Sati P, Nair G, Cortese ICM, Jacobson S, Smith BR, et al. Paramagnetic Rim Lesions are Specific to Multiple Sclerosis: An International Multicenter 3T MRI Study. Ann Neurol. 2020 Nov;88(5):1034–42. doi:10.1002/ana.25877 PubMed PMID: 32799417.

52. Weber CE, Wittayer M, Kraemer M, Dabringhaus A, Bail K, Platten M, et al. Long-term dynamics of multiple sclerosis iron rim lesions. Multiple Sclerosis and Related Disorders. 2022 Jan 1;57:103340. doi:10.1016/j.msard.2021.103340

Figures Legends

Figure 1 - Inclusion Criteria Flow Chart

Figure 2 - Lesion-Age Analysis

(A) Longitudinal lesion behavior of PRL (blue) and non-PRL (orange) over lesion age. Lines represent estimated slopes from a repeated-measures mixed-effects model with random intercepts for participants and lesions. (**B)** Comparison of lesion age between short-T1 and long-T1 non-PRL, based on a cross-sectional mixed-effects model with a random participant-level intercept. (**C)** Comparison of lesion age between short-T1 and long-T1 PRL, based on a cross-sectional mixed-effects model with a random participant-level intercept. (**D)** Examples of a short-T1 PRL (lesion age 1.1yrs, mean T1=1421ms) and long-T1 PRL (lesion age 3.2yrs, mean T1=1608ms) in a 26-year-old male with relapsing-remitting MS.

Figure 3 - Lesion volume distribution over different sNfL z-score groups

Bar plots indicate median and standard deviation, while the pie charts show mean lesional measures per z-score group.

Figure 4 - Treatment Analysis

(A) Observed longitudinal T1 time trajectories for untreated (blue) and anti-CD20–treated (yellow) lesions, stratified by lesion type. **(B–E)** Model-based predicted T1 time trajectories derived from a repeated-measures mixed model with a significant four-way interaction (Follow-up × Treatment × Lesion Type × T1 status). Panels show: **B** short-T1 non-PRL, **C** short-T1 PRL, **D** long-T1 non-PRL, and **E** long-T1 PRL lesions, illustrating subgroup-specific treatment effects.

Figure 5 - Working hypothesis of the association of PRL heterogeneity, clinical disability, neurofilament light chain, and treatment responsiveness. Following closure of the blood–brain barrier, T1 times increase within PRL, reflecting progressive tissue damage. This progression reflects ongoing demyelination and axonal degeneration, leading to release of NfL, particularly during the early stages of lesion development. In later stages, cumulative tissue injury is associated with greater clinical disability. Responsiveness of PRL to anti-CD20 antibody therapy decreases with increasing tissue T1, underscoring the importance of early therapeutic intervention during lesion evolution.

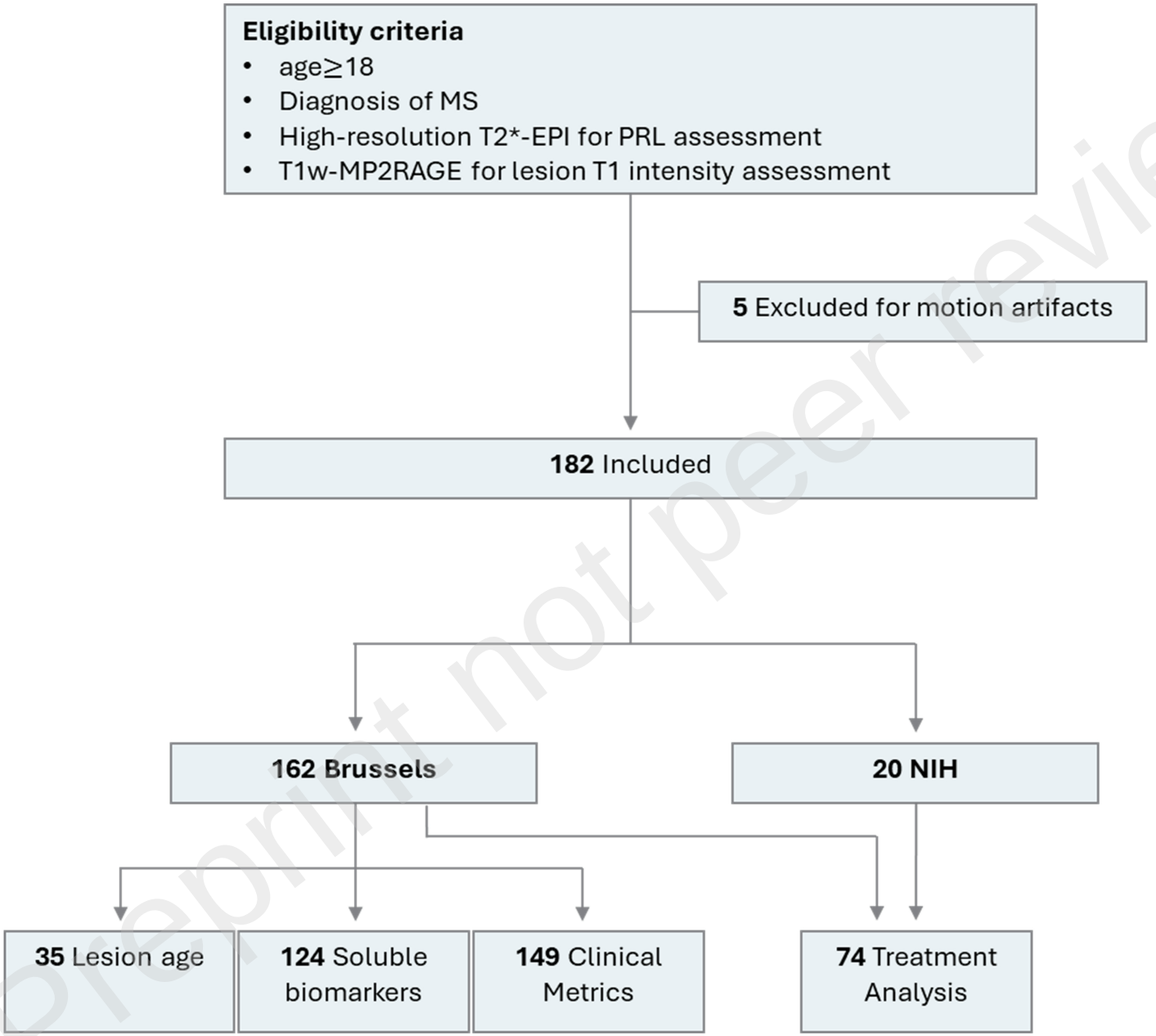

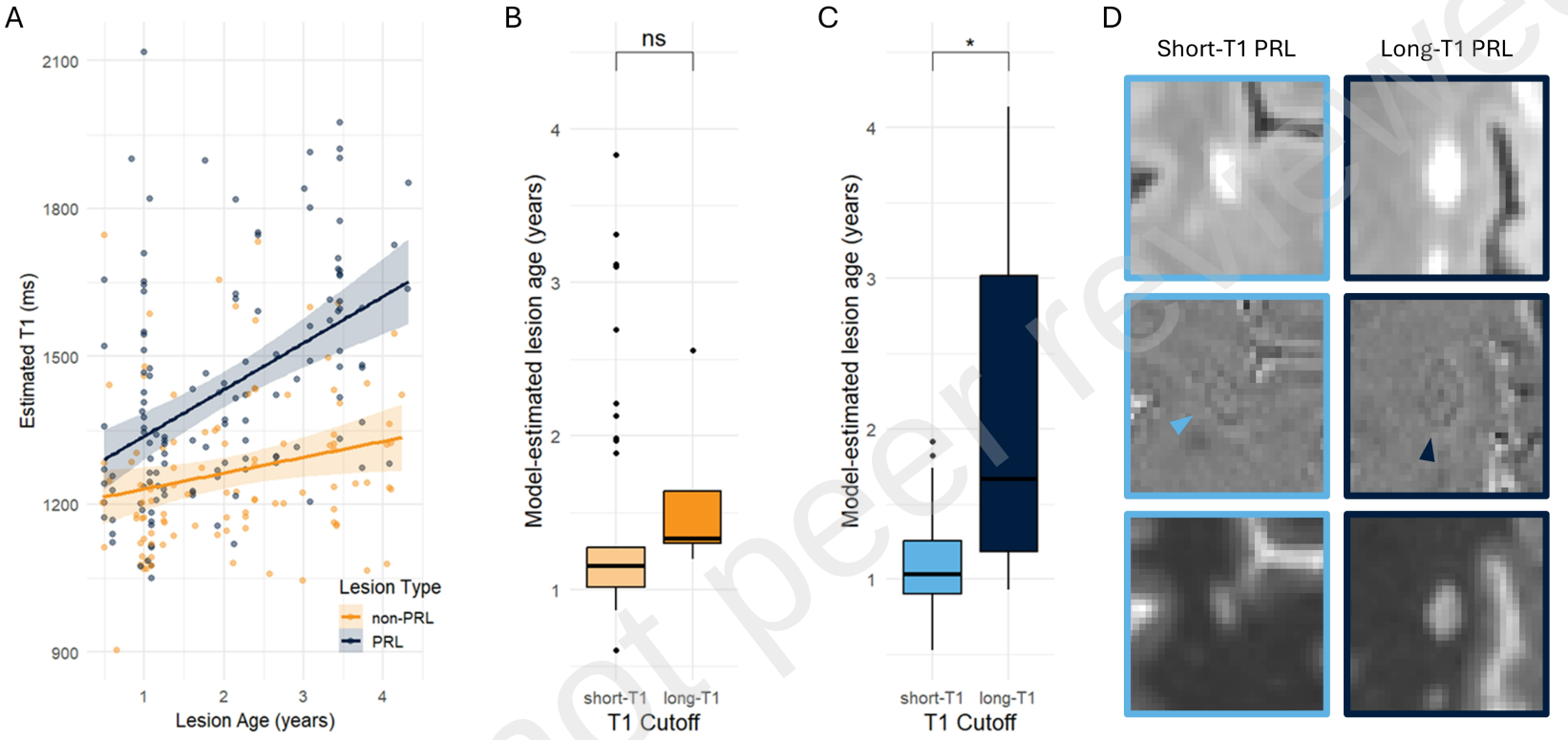

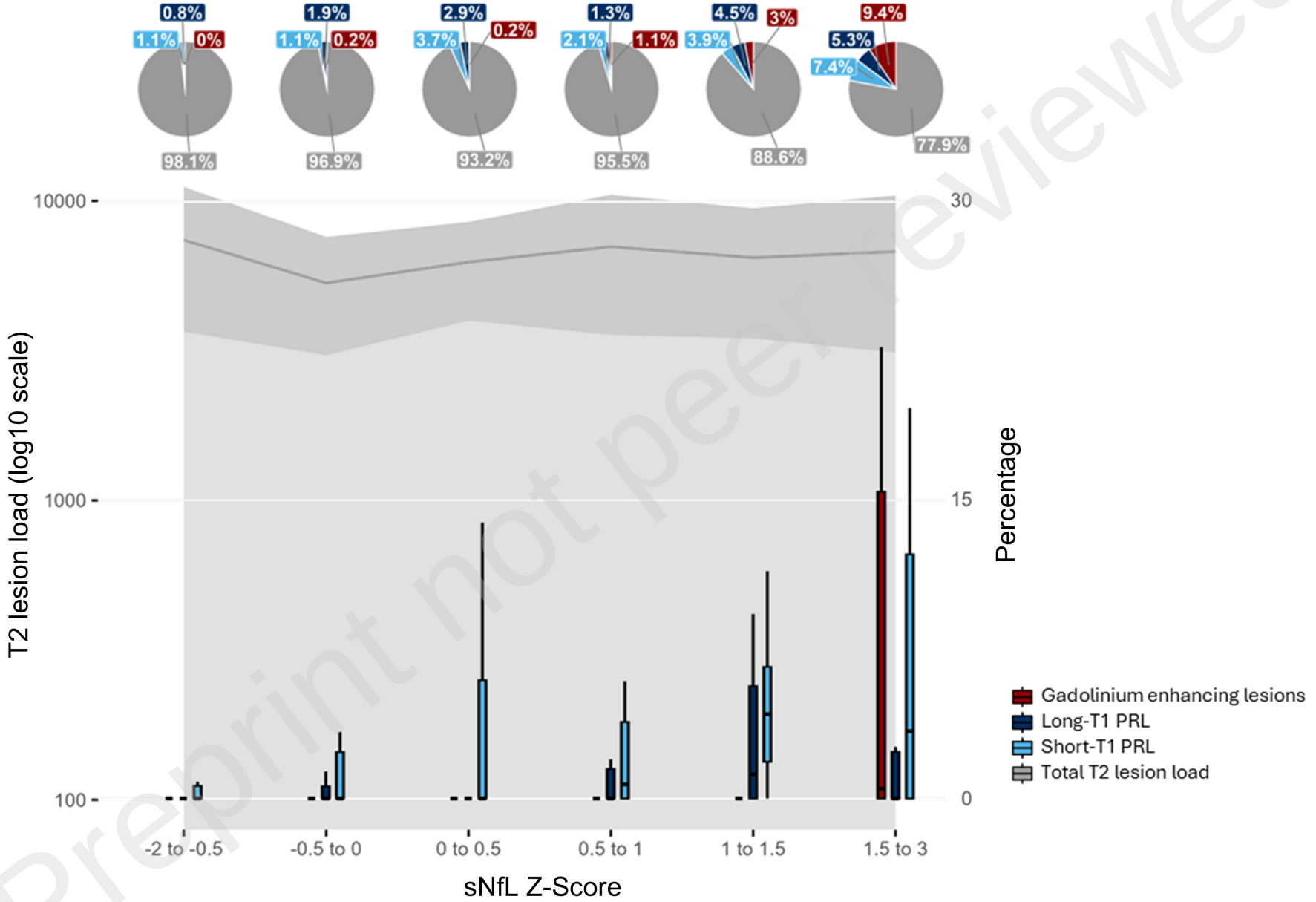

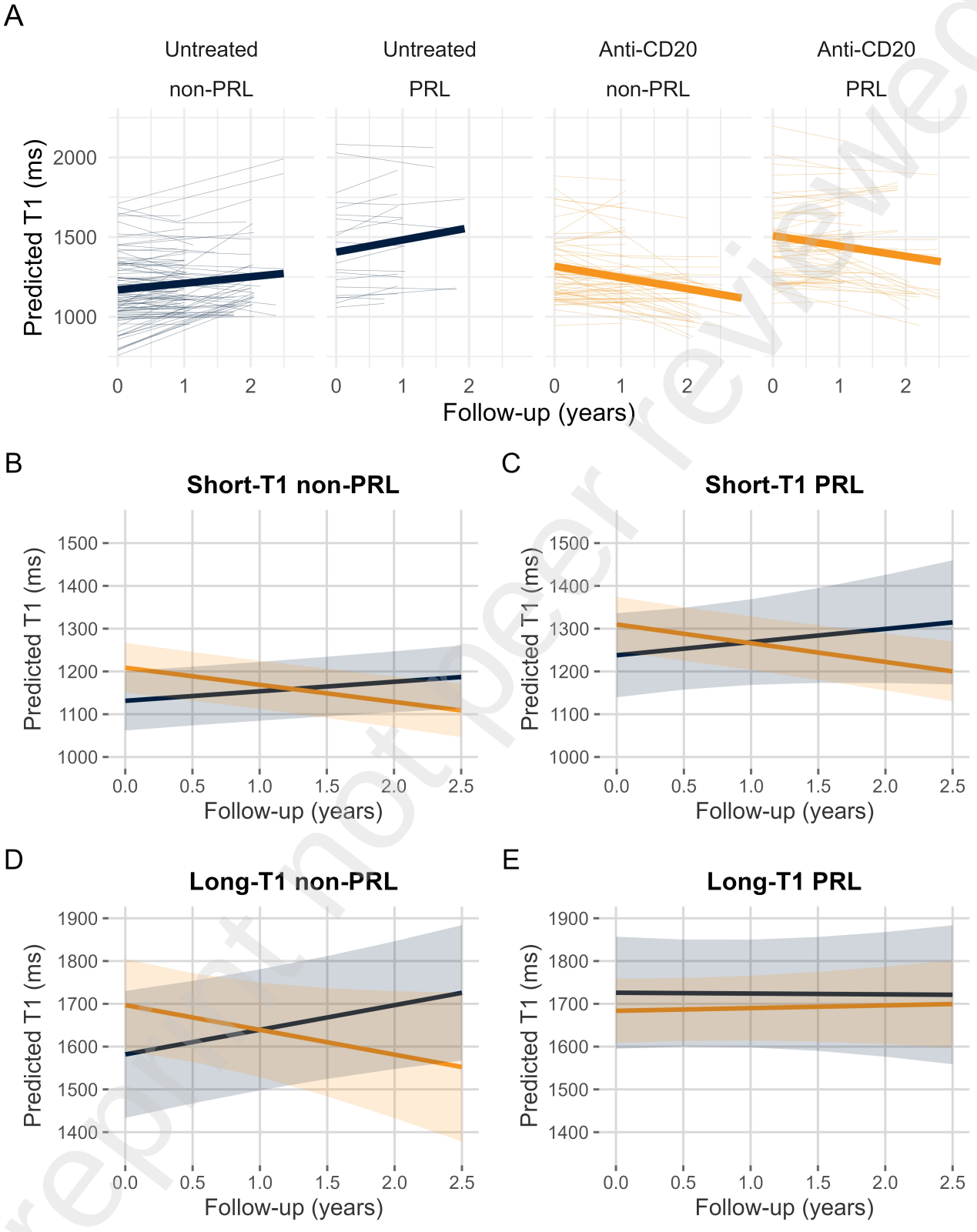

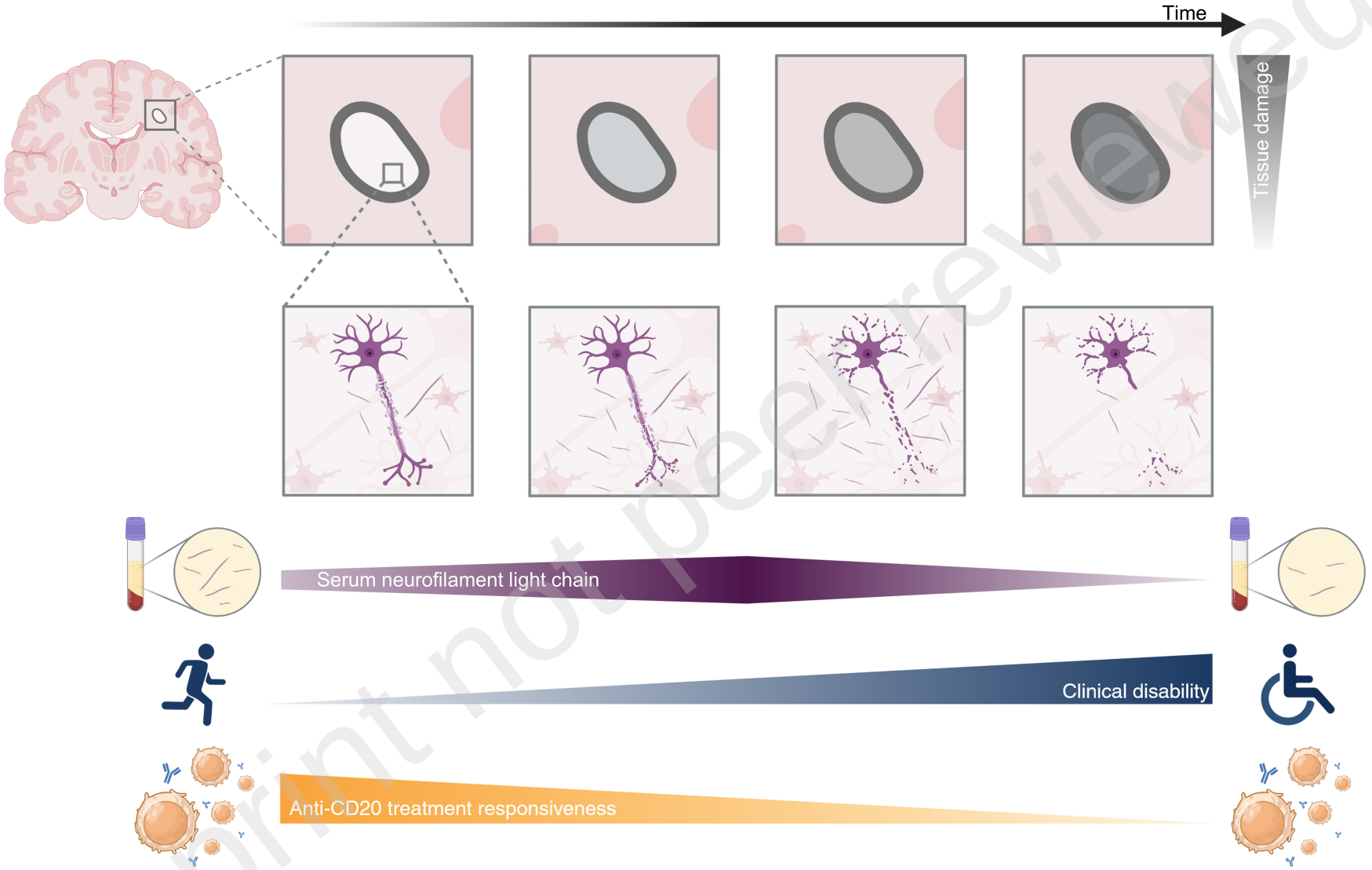

Table 1 - Demographic Data

	Overall, N = 182[a]	**NIH**, N = 20[a]	**Brussels**, N = 162[a]
Age (years)	44.11 ± 12.72	50.00 ± 13.01	43.38 ± 12.53
Sex			
Male	66 (36%)	7 (35%)	59 (36%)
Female	116 (64%)	13 (65%)	103 (64%)
Disease phenotype			
RRMS	124 (68%)	10 (50%)	114 (70%)
PMS	58 (32%)	10 (50%)	48 (30%)
EDSS	2.50 (0.00 – 8.00)	3.50 (0.00 – 8.00)	2.00 (0.00 – 7.00)
Norm. brain volume			0.74 (0.63 – 0.83)
T2LL (mm3)			5,012 (150 – 45,998)
PRL count	1 (0 – 84)	1 (0 – 10)	1 (0 – 84)
Long-T1 PRL count	0 (0 – 48)	0 (0 – 5)	0 (0 – 48)
Short-T1 PRL count	0 (0 – 36)	0 (0 – 5)	0 (0 – 36)
sNfL (Z-score)			0.22 (-1.70 – 3.89)

[a] Mean ± SD; n (%); Median (Range)

Abbreviations: EDSS: Expanded Disability Status Scale, RRMS: Relapsing-remitting Multiple Sclerosis; MS: Progressive Multiple Sclerosis; PRL: Paramagnetic rim lesions, sNfL: soluble neurofilament light chain, T2LL: T2 lesion load,